










Why thermal laser epitaxy aluminum sources yield reproducible fluxes in oxidizing environments

Cite as: J. Vac. Sci. Technol. A 41, 042701 (2023); doi: 10.1116/6.0002632

Submitted: 2 March 2023 · Accepted: 18 April 2023 ·

Published Online: 8 May 2023



Thomas J. Smart,¹  Felix V. E. Hensling,^{1,2,a)}  Dong Yeong Kim,¹  Lena N. Majer,¹  Y. Eren Suyolcu,²  Dominik Dereh,¹ Darrell C. Schlom,^{2,3,4}  Debdeep Jena,^{2,4,5}  Jochen Mannhart,¹  and Wolfgang Braun^{1,b)} 

AFFILIATIONS

¹Max Planck Institute for Solid State Research, Heisenbergstraße 1, Stuttgart 70569, Germany

²Department of Materials Science and Engineering, Cornell University, Ithaca, New York 14853

³Leibniz-Institut für Kristallzüchtung, Max-Born-Str. 2, Berlin 12489, Germany

⁴Kavli Institute at Cornell for Nanoscale Science, Cornell University, Ithaca, New York 14853

⁵School of Electrical and Computer Engineering, Cornell University, Ithaca, New York 14853

Note: This paper is a part of the Special Topic Collection: Papers from the 36th North American Conference on Molecular Beam Epitaxy (NAMBE 2022).

a) Author to whom correspondence should be addressed: f.hensling@fkf.mpg.de

b) Electronic mail: w.braun@fkf.mpg.de

ABSTRACT

Aluminum plays a central role in the world of electronic oxide materials. Yet, aluminum sources are very difficult to handle during oxide molecular-beam epitaxy, the main reason for which is the high oxidization potential of aluminum. In this work, we present a thorough study of the behavior of aluminum sources during oxide thermal laser epitaxy. We identify two distinct operating regimes. At high laser-beam fluences, the source emanates reproducible fluxes independent of an applied oxygen pressure of $< 10^{-1}$ hPa. At lower beam fluences, the flux increases with increasing oxygen pressure ($< 10^{-1}$ hPa) due to suboxide formation. We demonstrate reproducible rate control over a flux range of 5 orders of magnitude, which can be expanded further. These results demonstrate that thermal laser epitaxy does not present the challenges associated with the evaporation of aluminum during oxide molecular-beam epitaxy.

© 2023 Author(s). All article content, except where otherwise noted, is licensed under a Creative Commons Attribution (CC BY) license (<http://creativecommons.org/licenses/by/4.0/>). <https://doi.org/10.1116/6.0002632>

MAIN TEXT

The importance of oxides in the broad scope of electronic applications has become increasingly clear.^{1,2} Oxides comprising aluminum have played a specific and crucial role in this development. Sapphire, the most stable binary oxide of aluminum, is a substrate in rapidly increasing demand due to its low cost, superior properties over silicon, and high-quality wafer availability.³ Sapphire is also a material of interest for power electronics.^{4,5} Furthermore, several ternary aluminates have played a central role in some of the most exciting discoveries in the field of oxides. Examples of this are the development of freestanding single-crystal perovskite films enabled by sacrificial $\text{Sr}_3\text{Al}_2\text{O}_6$ layers⁶ and two-dimensional electron gas at the interface of LaAlO_3 and SrTiO_3 .^{7,8}

Molecular-beam epitaxy (MBE) is considered the “gold standard” for the growth of oxides and most electronic materials. The achievable purity, mobility, structural perfection, and atomic control are unmatched by any other technique.^{9,10} Despite the central role of aluminum in the field of oxides and the importance of oxide MBE, the operational instability of aluminum effusion-cell sources has remained a longstanding challenge. The instability of aluminum effusion cells is illustrated in Fig. 1(a). Aluminum has a high oxidization potential, and Al_2O_3 has an extremely low vapor pressure.¹¹ Therefore, aluminum species react with the oxygen species of the growth atmosphere and deposit Al_2O_3 at the cell’s neck. This results in the so-called choking of the cell—a constant decrease in the flux until no aluminum emanation takes place.

There have been numerous attempts to develop a solution to this issue. For example, the recently presented suboxide MBE (s-MBE) has yielded promising results for other group-III oxides with regard to achievable crystal quality, growth speed, and flux stability.^{12–14} However, aluminum suboxide effusion cells retain the undesired flux instability known from their metal counterparts. This is illustrated by the decrease in the adatom flux as a function of time measured with a quartz crystal microbalance in Fig. 1(b). This is probably caused by further oxidization of the suboxide like that observed for silicon suboxide sources.^{15,16}

We will show that thermal laser epitaxy (TLE)¹⁷ meets the challenge of supplying a reproducible aluminum flux in an oxidizing environment. To present the underlying mechanism, we first provide an in-depth analysis of the source's interaction with the heating laser beam as well as with the oxide environment and then proceed to explore the limits of this new technique.

TLE has recently emerged as a promising approach to the issues stated above. It features a wider parameter space for epitaxial growth than any other deposition technique. As the name suggests, TLE is based on thermally evaporating a source by locally heating it with a continuous-wave laser. This makes in-chamber electronics obsolete, and thus allows—as we will show in this work—much higher background gas pressures than conventional physical deposition techniques.¹⁷ Not long after its development, TLE's potential for oxide epitaxy was achieved.^{18,19} Here, we will investigate in detail the behavior of the aluminum source operated in an oxygen environment.

The cross section of the TLE chamber in which these experiments were performed is shown in Fig. 2. The chamber was operated without substrate heating and was water-cooled to 17°C to dissipate reflected laser radiation. Source heating was provided by a fiber-coupled disk laser with $\lambda = 1030$ nm and a peak power of 500 W for experiments with oxygen background pressure and a fiber-coupled disk laser with $\lambda = 1030$ nm and a peak power of 2000 W for experiments in UHV. The laser spot size upon the source was approximately 1 mm² with an approximate Gaussian profile. The distance between the focus of the laser and the source equaled 130 mm. Deposition was performed on $10 \times 10 \times 0.5$ mm³ Si(111) substrates. The high-purity aluminum metal (4N5) was placed in a sapphire crucible and loaded onto a manipulator arm driven by linear motors attached to the x and y directions, allowing a circular motion of the laser spot on the source as illustrated in Fig. 2. O₂ was used as an oxidizing agent. The applied oxygen pressure was varied between 10^{-4} and 10^{-1} hPa. For each pressure setting, the incident laser power was also varied. The resulting film thickness was measured by a profilometer, and the growth rate was determined accordingly. For each experiment, a new source was used and pre-melted with ≈ 30 W incident laser power under UHV conditions to test, ensure reproducibility, and eliminate impurities.

Figure 3 shows photographs of the aluminum source in a 10^{-3} hPa oxygen environment at 120 W (top) and 300 W (bottom) laser power with (right) and without (left) a circular motion of the source. At low laser powers, the source material coalesces into a sphere, see Figs. 3(a) and 3(b). Furthermore, the formation of a white oxide crust is observable. At lower laser powers without applied motor motion, this crust forms everywhere but at the laser

spot, see Fig. 3(a). In the case of a circular motion, the area without oxide formation increases to match the laser spot motion at low laser powers, see Fig. 3(b). At higher laser powers, the effects of the beam motion vanish, and the area without oxide crust formation becomes much larger than the laser spot, see Fig. 3 (bottom). The coalescence of the source is diminished.

The formation of the source's spherical shape is directly related to the appearance of the oxide crust. At first, the Al coalescence is driven by the strong cohesion of the liquid metal²⁰ and by

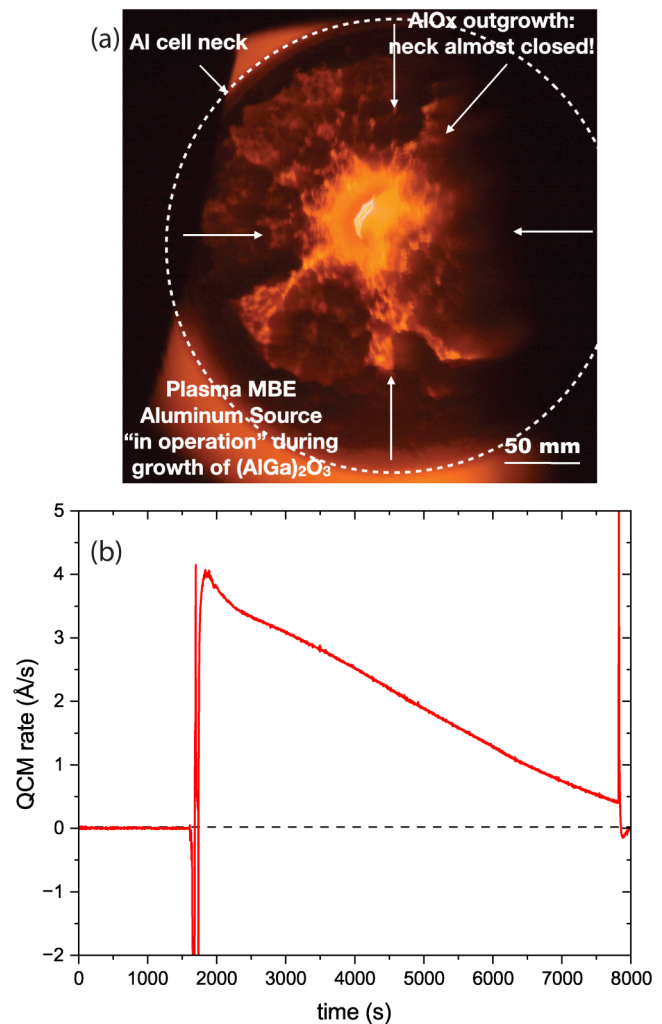


FIG. 1. (a) *In operando* photograph of an aluminum effusion cell during $\text{Al}_{2-x}\text{Ga}_x\text{O}_3$ growth, taken from the substrate's point of view. It clearly shows the outgrowth of Al_2O_3 from the cell's neck that is slowly choking off the aluminum flux. At this point, the flux is already significantly reduced, and soon, aluminum will no longer emanate. (b) Decrease in the flux over time for an aluminum suboxide source measured with a quartz crystal microbalance. The two extreme oscillations at the end and beginning of the flux measurement result from interference when operating the shutter.

Downloaded from http://pubs.aip.org/avs/jvst/article-pdf/doi/10.1116/6.0002632/17408919/042701_1_6.0002632.pdf

the small adhesion to the oxygen-terminated Al₂O₃ surface of the crucible, which causes a large contact angle. In the absence of oxygen, it is expected that, upon further heating of the aluminum source, the contact angle between source material and crucible decreases. This is due to the decreasing surface tension²¹ and a decreasing wetting angle caused by the formation of a higher-energy metallic surface reconstruction of the sapphire crucible.²² This is indeed found for high fluences of the laser beam, see Fig. 3 (bottom). However, for low fluences, the formation of the oxide crust prevents the equilibrium contact angle that is expected to be reached between the metallic aluminum source material and the crucible. The spherical shape of the molten Al is, therefore, maintained.

From the photographs in the top row of Fig. 3, it is evident that only a small portion of the source surface is comprised of metallic aluminum (dark) and that most of the oxide crust is intact (bright). The metallic surface part of the source coincides with the laser spot, Fig. 3(a), and with the path of the circular motion of the source, Fig. 3(b), for the cases of resting and moving sources, respectively. However, the non-oxidized surface area is much bigger and independent of the source motion in the higher power regime. To investigate whether these two source behavior regimes impact the resulting adatom flux, we compared the growth rate as a function of laser power. We consider the case of a resting source (no motion) in UHV (purple & triangles) under 10⁻³ hPa oxygen background pressure (blue & squares), and the case of a source motion on a circular track of 1 mm diameter under 10⁻³ hPa oxygen background pressure (red & circles), Fig. 4. As neither Al, Al₂O, nor Al₂O₃ are volatile at room temperature,¹¹ and as the substrate is not heated intentionally, the growth rate is a direct measure of the flux. In UHV (purple & triangles), the growth rate indeed shows the expected Arrhenius-type dependence on the beam fluence.²³ In the presence of an oxygen background pressure, the growth rate is characterized by two laser-power-dependent regimes that match the regimes (top and bottom) observed in

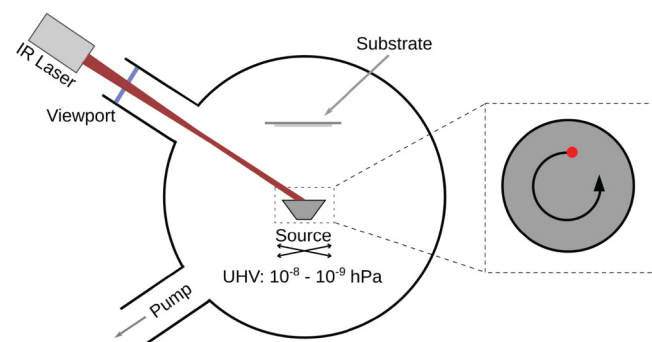


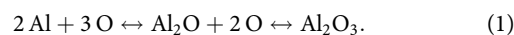
FIG. 2. Illustration of the TLE chamber used to investigate the evaporation behavior of Al in an O₂ atmosphere. The source is moved along a circular path by a pair of motors attached to the manipulator arm on which the source rests. The laser scans the surface of the source along a circular path with a radius of 1 mm. The laser we used here is a $\lambda = 1030$ nm disk laser with a peak power of 500 W. The source–substrate distance was kept at 60 mm.

Fig. 3. For a laser output power of > 220 W, the growth rate is independent of a possible source motion. As a function of laser power, it shows the Arrhenius behavior of a source operated in UHV. For laser output powers < 220 W, the slope of the growth rate as a function of laser power is more shallow than in the UHV regime, revealing in this case that the formation of the oxide crust plays a central role in the emanating flux. The flux is also much higher for an applied circular motion of the source, implying that an increased non-oxidized surface results in an increased flux. In fact, the increase in flux is proportional to the non-oxidized area as controlled by the applied radius of the circular motion. The top row of Fig. 3 shows an increase in the exposed surface area by a factor of ≈ 10 (from 1.4 to 13 mm²) and Fig. 4 reveals an increase in the growth rate upon circular source motion by the same factor (from 0.1 to 1 Å/s).

The behavior of the source in the high laser-power regime (> 220 W) can be easily understood. The source is sufficiently heated to shift the thermodynamic equilibrium away from oxidizing conditions. This is why the source in this regime looks like previously reported aluminum TLE sources in UHV.^{23,24} It can be assumed that the entire source area contributes to the aluminum evaporation, which is why the applied motion no longer plays a role. Thus, it is not surprising that the evaporation behavior follows the established Arrhenius law for the dependence of aluminum sources in UHV on laser power.^{23,24} The wide range of available growth rates is worth mentioning in this context. Depending on the applied laser power and the application of a source motion, a growth rate variation over 5 orders of magnitude can be induced with a laser power variation of just over 1 order of magnitude. This deposition regime constitutes the regime with the highest reproducibility.

To understand the more complex behavior of the source in the low laser-power regime (< 220 W), we investigated the flux dependence on the laser power for a wider range of applied oxygen pressures. Figure 5 illustrates this dependence for oxygen pressures between 10⁻⁴ and 10⁻¹ hPa and sources moving in a circle with a radius of 1 mm. For orientation purposes, the expected Arrhenius dependence of the growth rate on laser power for the evaporation of a source in UHV is marked by a purple dashed line. For the lowest oxygen pressure of 10⁻⁴ hPa (green & diamonds), the flux follows the Arrhenius behavior of a non-oxidized source down to relatively low laser powers (≈ 165 W). This is in agreement with the less oxidizing conditions. Counterintuitively, the flux in the lower laser-power regime increases with increasing oxygen pressure up to 10⁻² hPa. For pressures $\geq 10^{-1}$ hPa, the flux decreases again.

To account for this behavior, it is important to consider the two-step oxidation reaction for group-III elements,^{13,14,25–27}



Under oxidizing conditions, aluminum can, thus, be present in one or more of the three phases Al₂O₃, Al₂O, and Al. We have established above that no significant source oxidation takes place at higher laser powers, and the flux is dominated by the evaporation of metallic Al. As the oxidation potential increases with decreasing temperature, we observe that an oxide crust forms to coat Al, see Fig. 3 (top). Considering the low vapor pressure of Al₂O₃, it is

Downloaded from http://pubs.aip.org/avs/journal-article-pdf/doi/10.1116/6.0002632/174089191042701_1_6.0002632.pdf

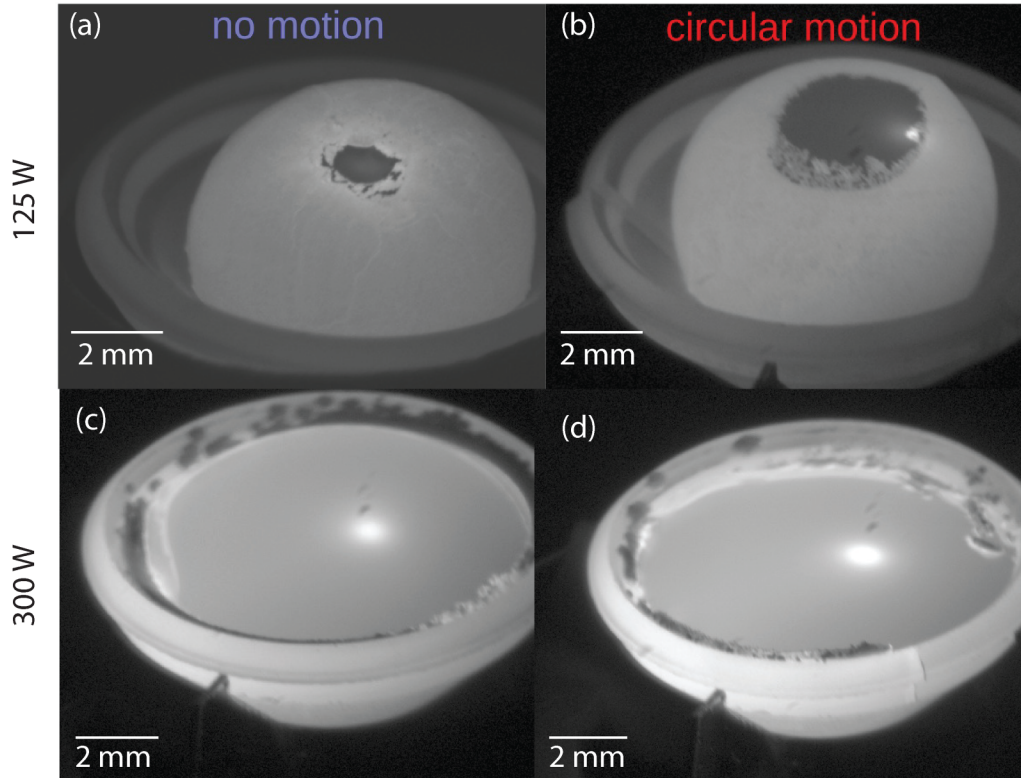


FIG. 3. Photographs of the oxidized Al source in 10^{-3} hPa oxygen at 120 W [(a) and (b)] and 300 W [(c) and (d)] with no circular motion [(a) and (c)] and circular motion with a radius of 1 mm [(b) and (d)].

unlikely that the oxide crust itself contributes a significant flux. However, the suboxide Al_2O may also be present. It is well known for metals that form suboxides with much higher vapor pressures (Sn, Ga) that a significant contribution to the flux arises from the suboxide formation. This behavior was first reported for oxide MBE.²⁸ At sufficiently high temperatures (> 1600 K), the vapor pressure of Al_2O is, in fact, greater than the vapor pressure of metallic Al.^{11,24} Considering the high local temperature of the source in TLE, the suboxide of aluminum has to be expected to contribute significantly to the resulting flux, much like the behavior of high-vapor-pressure oxides in oxide MBE.^{24,28} The obvious explanation for the increase in flux with an increase in oxygen pressure is, therefore, the increased formation of Al_2O , which sublimates immediately after its formation and increases the flux.

This explanation can be probed by calculating the maximum suboxide flux achievable at a fixed pressure (10^{-2} , 10^{-3} , 10^{-4} hPa) and comparing it to the observed growth rates. The formation of suboxide on the target surface is naturally limited by the impinging O-flux j_{O} , which can be calculated by using kinetic gas theory,^{28,29}

$$j_{\text{O}} = 2p_{\text{O}_2} \left(\frac{N_A}{2\pi mk_B T} \right)^{1/2}, \quad (2)$$

where p_{O_2} is the applied oxygen pressure, N_A is the Avogadro constant, m is the molecule mass, and T is the gas temperature, which we assumed to be 300 K. The flux j_{O} obtained from Eq. (2) can then be used to obtain the expected maximum flux of suboxide at the substrate under geometric considerations,^{28,29}

$$j_{\text{Al}_2\text{O}, \text{max}} = \frac{r^2}{L^2} \cos(\Phi) \times j_{\text{O}}. \quad (3)$$

We assume our source radius r as the radius of the circular path of the source (1 mm), the distance between target and substrate is $L = 60$ mm, and the angle between source Φ and substrate is close to 0° . The resulting maximum suboxide fluxes for the pressures 10^{-2} , 10^{-3} , and 10^{-4} hPa are converted into growth rates and marked by the horizontal dashed lines in Fig. 5. The good agreement between the predicted maximum suboxide growth rate and the observed growth rate further underlines that the observed increase in the growth rate with an increase in the oxygen pressures is indeed a result of Al_2O formation and sublimation.

This behavior changes at 10^{-1} hPa oxygen background pressure. At low laser powers, the growth rate no longer increases with increasing laser power or increasing oxygen pressure. At higher laser powers (> 140 W), we observe that the growth stops (gray

Downloaded from http://pubs.aip.org/avs/journal-article-pdf/doi/10.1116/1.5002632/17408919042701_1_6.0002632.pdf

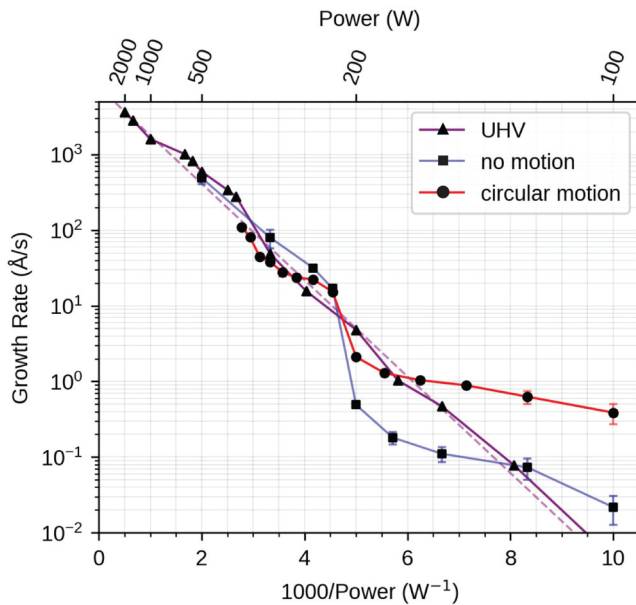


FIG. 4. Measured growth rate of films by deposition of adatoms emanating from an aluminum source as a function of laser power in UHV (purple & triangles) with an applied O_2 background pressure of 10^{-3} hPa (blue & squares) for a resting source and with an O_2 pressure of 10^{-3} hPa for a source on a circular motion path with a radius of 1 mm (red & circles). The dashed line represents the expected Arrhenius-like dependence of the growth rate on the laser power for an aluminum source in UHV.

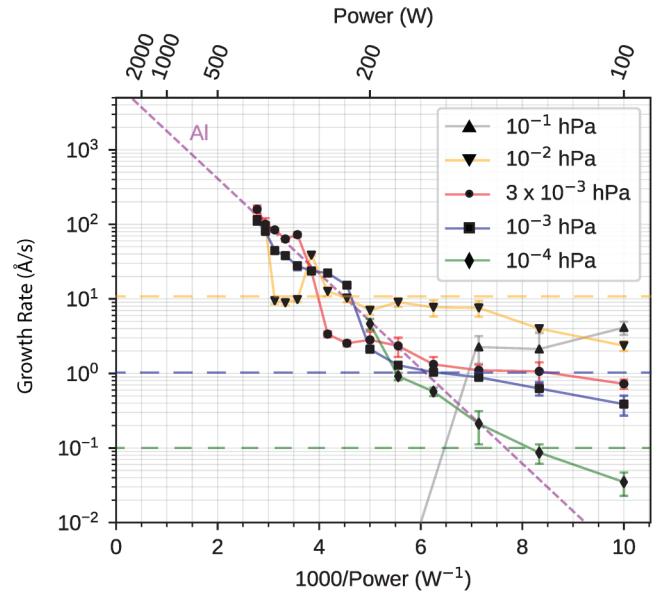


FIG. 5. Measured rate of film growth achieved by evaporating an aluminum source in an O_2 atmosphere within a range of O_2 pressures. The purple dashed line indicates the Arrhenius-like dependence of the growth rate of Al in UHV as a function of incident laser power. The horizontal dashed lines represent the calculated maximal suboxide flux at the respective pressures. Each source was moved on a circular path with a radius of 1 mm.

line in Fig. 5). Studying the source after growth at high pressures and high laser powers provides a clue to explaining this behavior. Figure 6 shows an optical microscopy image of the source after being exposed to 10^{-1} hPa at 300 W of incident laser power. Al_2O_3 crystals formed on the surface of the source are well visible. We conclude that, at 10^{-1} hPa oxygen pressure, the oxidation

potential becomes so high that oxidation is favorable even at extremely high temperatures (locally > 2000 K). As a result in the low laser-power regime, less suboxide can contribute to the flux because more Al_2O_3 is formed. In the high laser-power regime, the energy supplied by the laser is even sufficient to promote the growth of Al_2O_3 single crystals. As a result, the source stops emanating particles.

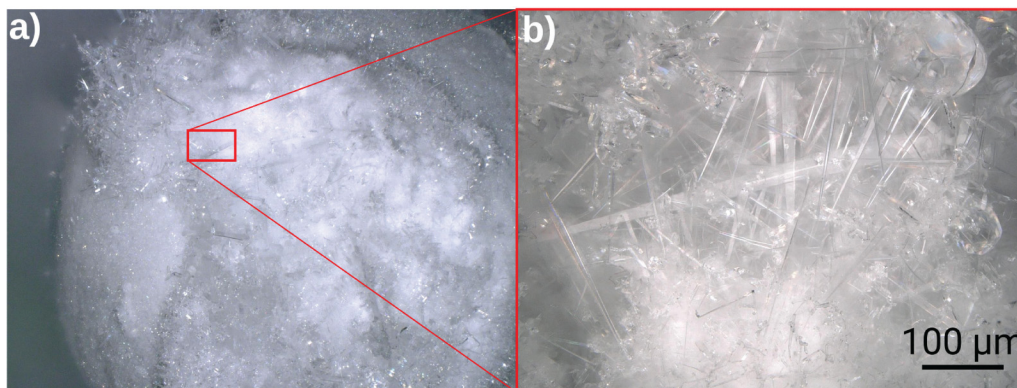


FIG. 6. (a) Optical microscopy image of a heavily oxidized Al source after using it for 10 min with 300 W of incident laser power and 10^{-1} hPa oxygen pressure. (b) Zoom-in revealing single-crystal dendrites of Al_2O_3 on the surface of the source.

Downloaded from http://pubs.aip.org/avs/journal-article-pdf/doi/10.1116/6.0002632/17408919042701_1_6.0002632.pdf

In summary, we have provided a systematic study of the behavior of aluminum sources used in thermal laser epitaxy under oxidizing conditions. We find that, for laser powers above 220 W and illuminated areas of 1 mm², a reproducible flux is achieved for oxygen pressures up to 10⁻² hPa. This exhibits an Arrhenius-law-type dependence as a function of laser output power. We found an upper limit of oxygen pressure useful for film growth on the order of 10⁻² hPa. At higher pressures, the source oxidizes and becomes unusable. For laser powers below 220 W, the adatom flux is a function of the applied oxygen pressure and the exposed surface area of the source. In this regime, due to the formation of Al₂O, the flux increases proportionally to the oxygen flux reaching the exposed source area. By virtue of these mechanisms, TLE can be applied to vary the adatom flux emanating from Al sources over a range unmatched by any other technique. (Note that 5 orders of magnitude of growth rates were demonstrated here.) We expect that this in-depth understanding of the operating regimes of aluminum sources in TLE will pave the way for high-quality sapphire epitaxy. Furthermore, by identifying the oxygen-independent high laser-power regime, we expect that TLE can be applied to grow aluminum-based ternaries.

ACKNOWLEDGMENTS

The authors thank Varun Harbola and Sander Smink for many insightful discussions. The authors also thank Fabian Felden, Ingo Hagel, Konrad Lazarus, Sabine Seiffert, and Wolfgang Winter for technical support.

AUTHOR DECLARATIONS

Conflict of Interest

The authors have no conflicts to disclose.

Author Contributions

Thomas J. Smart: Conceptualization (equal); Data curation (lead); Formal analysis (lead); Investigation (lead); Methodology (lead); Supervision (supporting); Writing – original draft (equal); Writing – review & editing (equal). **Felix V. E. Hensling:** Conceptualization (equal); Formal analysis (equal); Investigation (equal); Methodology (equal); Supervision (equal); Writing – original draft (equal); Writing – review & editing (equal). **Dong Yeong Kim:** Formal analysis (equal); Investigation (supporting); Methodology (supporting); Writing – review & editing (supporting). **Lena N. Majer:** Data curation (supporting); Formal analysis (supporting); Investigation (supporting). **Y. Eren Suyolcu:** Data curation (supporting). **Dominik Dereh:** Data curation (equal). **Darrell Schlom:** Investigation (supporting); Methodology (supporting); Supervision (supporting). **Debdeep Jena:** Conceptualization (supporting); Data curation (supporting). **Jochen Mannhart:** Conceptualization (supporting); Funding acquisition (lead); Investigation (supporting); Methodology (supporting); Project

administration (equal); Supervision (equal); Writing – review & editing (lead). **Wolfgang Braun:** Conceptualization (equal); Data curation (equal); Formal analysis (equal); Investigation (equal); Methodology (equal); Supervision (equal); Writing – review & editing (equal).

DATA AVAILABILITY

The data that support the findings of this study are available within the article and from the corresponding author upon reasonable request.

REFERENCES

- 1 M. Lorenz *et al.*, *J. Phys. D: Appl. Phys.* **49**, 433001 (2016).
- 2 M. Coll *et al.*, *Appl. Surf. Sci.* **482**, 1 (2019).
- 3 M. S. Akselrod and F. J. Bruni, *J. Cryst. Growth* **360**, 134 (2012).
- 4 R. Jinno *et al.*, *Sci. Adv.* **7**, eabd5891 (2021).
- 5 H. Okumura, *Jpn. J. Appl. Phys.* **61**, 125505 (2022).
- 6 D. Lu, D. J. Baek, S. S. Hong, L. F. Kourkoutis, Y. Hikita, and H. Y. Hwang, *Nat. Mater.* **15**, 1255 (2016).
- 7 A. Ohtomo and H. Y. Hwang, *Nature* **427**, 423 (2004).
- 8 N. Nakagawa, H. Y. Hwang, and D. A. Muller, *Nat. Mater.* **5**, 204 (2006).
- 9 D. G. Schlom, *APL Mater.* **3**, 062403 (2015).
- 10 Y. E. Suyolcu, G. Christiani, P. A. van Aken, and G. Logvenov, *J. Supercond. Novel Magn.* **33**, 107 (2020).
- 11 K. M. Adkison, S.-L. Shang, B. J. Bocklund, D. Klimm, D. G. Schlom, and Z.-K. Liu, *APL Mater.* **8**, 081110 (2020).
- 12 F. V. E. Hensling, M. A. Smeaton, V. Show, K. Azizie, M. R. Barone, L. F. Kourkoutis, and D. G. Schlom, *J. Vac. Sci. Technol. A* **40**, 062707 (2022).
- 13 P. Vogt *et al.*, *APL Mater.* **9**, 031101 (2021).
- 14 P. Vogt, D. G. Schlom, F. V. E. Hensling, K. Azizie, Z.-K. Liu, B. J. Bocklund, and S.-L. Shang, “Suboxide molecular-beam epitaxy and related structures,” U.S. patent 11,462,402 (October 4, 2022).
- 15 A. Ardenghi, O. Bierwagen, A. Falkenstein, G. Hoffmann, J. Lähnemann, M. Martin, and P. Mazzolini, *Appl. Phys. Lett.* **121**, 042109 (2022).
- 16 K. Azizie *et al.*, *APL Mater.* **11**, 041102 (2023).
- 17 W. Braun and J. Mannhart, *AIP Adv.* **9**, 085310 (2019).
- 18 D. Y. Kim, J. Mannhart, and W. Braun, *APL Mater.* **9**, 081105 (2021).
- 19 D. Y. Kim, J. Mannhart, and W. Braun, *J. Vac. Sci. Technol. A* **39**, 053406 (2021).
- 20 I. Egry, E. Ricci, R. Novakovic, and S. Ozawa, *Adv. Colloid Interface Sci.* **159**, 198 (2010).
- 21 D. B. Macleod, *Trans. Faraday Soc.* **19**, 38 (1923).
- 22 C. Barth and M. Reichling, *Nature* **414**, 54 (2001).
- 23 T. J. Smart, J. Mannhart, and W. Braun, *J. Laser Appl.* **33**, 022008 (2021).
- 24 D. Y. Kim, T. J. Smart, L. Majer, S. Smink, J. Mannhart, and W. Braun, *J. Appl. Phys.* **132**, 245110 (2022).
- 25 P. Vogt and O. Bierwagen, *Phys. Rev. Mater.* **2**, 120401(R) (2018).
- 26 P. Vogt and O. Bierwagen, *Appl. Phys. Lett.* **106**, 081910 (2015).
- 27 P. Vogt and O. Bierwagen, *Appl. Phys. Lett.* **109**, 062103 (2016).
- 28 G. Hoffmann, Z. Cheng, O. Brandt, and O. Bierwagen, *APL Mater.* **9**, 111110 (2021).
- 29 S. Franchi and M. Heini, *Molecular Beam Epitaxy: From Research to Mass Production* (Elsevier, New York, 2013).